Journal of Applied Physics

Three-step growth of highly photoresponsive $BaSi_2$ light absorbing layers with uniform Ba to Si atomic ratios

Cite as: J. Appl. Phys. **126**, 215301 (2019); https://doi.org/10.1063/1.5128690
Submitted: 21 September 2019 . Accepted: 15 November 2019 . Published Online: 02 December 2019

Yudai Yamashita, Takuma Sato, Noriyuki Saitoh, Noriko Yoshizawa, Kaoru Toko, and Takashi Suemasu

Journal of Applied Physics ARTICLE scitation.org/journal/jap

Three-step growth of highly photoresponsive $BaSi_2$ light absorbing layers with uniform Ba to Si atomic ratios

Cite as: J. Appl. Phys. **126**, 215301 (2019); doi: 10.1063/1.5128690
Submitted: 21 September 2019 · Accepted: 15 November 2019 ·
Published Online: 2 December 2019

Yudai Yamashita,[1] Takuma Sato,[1,2] Noriyuki Saitoh,[3] Noriko Yoshizawa,[3] Kaoru Toko,[1] and Takashi Suemasu[1,a)]

AFFILIATIONS

[1]Institute of Applied Physics, University of Tsukuba, Tsukuba, Ibaraki 305-8573, Japan
[2]Université Grenoble Alpes, CEA, CNRS, IRIG, SyMMES, 38000 Grenoble, France
[3]Electron Microscope Facility, TIA, AIST, 16-1 Onogawa, Tsukuba, Ibaraki 305-8569, Japan

[a)]**Author to whom correspondence should be addressed:** suemasu@bk.tsukuba.ac.jp

ABSTRACT

Barium disilicide ($BaSi_2$) shows great promise as a light absorbing material for solar cell applications. Thus, it is important to form high-quality $BaSi_2$ films with a low defect density. We previously found that the photoresponsivity of *a*-axis-oriented $BaSi_2$ epitaxial films was enhanced drastically when formed under Si-rich conditions by molecular beam epitaxy. However, the degree of *a*-axis crystal orientation normal to the sample surface was degraded. In this work, we investigated the origin of this degradation by cross-sectional transmission electron microscopy (X-TEM). It was found that excess Si atoms in $BaSi_2$ films diffused out and precipitated around the $BaSi_2$/Si interface, resulting in the formation of Si layers with an interface roughness of 0.2–0.3 μm when grown under Si-rich conditions. Furthermore, extended defects stemming from such rough interface regions were detected by deep level transient spectroscopy, and they acted as hole trap defects. To achieve high photoresponsivity in $BaSi_2$ films under Si-rich conditions while avoiding such Si precipitation, we proposed a three-step growth method for $BaSi_2$ films. X-TEM observations confirmed uniform Ba to Si atomic ratios throughout the entire layer and smooth $BaSi_2$/Si interfaces. In addition, relative to films grown by the conventional two-step method, the *a*-axis orientation was improved significantly, and the photoresponsivity increased by approximately five times to reach 0.5 A/W at a wavelength of 800 nm under a bias voltage of −0.1 V. This corresponds to an external quantum efficiency above 90%.

I. INTRODUCTION

Development of solar cells with high conversion efficiency (η) is progressing in attempts to realize a low-carbon society. Crystalline-Si (c-Si) solar cells account for approximately 90% of the photovoltaics market. The η of c-Si has exceeded 26%[1] and is now approaching the theoretical limit of this material system.[2] Compound semiconductor solar cells, such as GaAs, have achieved higher η values than those in c-Si solar cells.[3] However, the practical use of GaAs-based solar cells is difficult because these materials are expensive and contain rare and/or toxic elements. Hence, there is a need to develop alternative thin-film solar cell materials. We have focused on semiconducting barium disilicide ($BaSi_2$)[4,5] because it is composed of safe, stable, and abundant elements. Furthermore, it possesses attractive features, such as a suitable bandgap for a single-junction solar cell (~1.3 eV), a high optical absorption coefficient of $\alpha = 3 \times 10^4$ cm^{-1} at 1.5 eV (more than 40 times larger than that of c-Si),[6–9] a large minority-carrier diffusion length ($L \approx 10\,\mu$m),[10] and bipolar doping properties.[11–14] $BaSi_2$ has a small lattice mismatch with Si(111), i.e., 0.1% and 1.1% along the *b*- and *c*-axes, respectively, allowing for epitaxial growth on an inexpensive Si substrate.[15] For these reasons, $BaSi_2$ is considered to be a promising material for solar cell applications. We have achieved η values approaching 10% in p^+-$BaSi_2$/n-Si heterojunction solar cells,[16–18] wherein the depletion region stretched toward the n-Si side and, therefore, most of the photons were absorbed in the n-Si region. Our next target is $BaSi_2$-pn homojunction solar cells, for which η is expected to exceed 25% according to calculations.[19] Recently, we reported the operation of homojunction solar cells; however, the η was quite limited.[20–22] To achieve solar cells with a

high η requires the formation of high-quality $BaSi_2$ light absorbers with a low defect density.

In our previous work, defect characterizations of $BaSi_2$ films were conducted using deep level transient spectroscopy (DLTS),[23,24] positron annihilation spectroscopy,[25] Raman spectroscopy,[26] and electron paramagnetic resonance,[27] wherein we detected vacancy-type defects, which we regard as Si vacancies (V_{Si}). First-principles calculations also show that V_{Si} are likely to occur in $BaSi_2$[14] and that these vacancies give rise to localized states within the bandgap. Therefore, reducing the density of V_{Si} is a present agenda to form high-quality $BaSi_2$ light absorbing layers. Recent studies have shown that the minority-carrier lifetime and photoresponsivity of $BaSi_2$ increased significantly by irradiation of atomic hydrogens onto $BaSi_2$ films.[28,29] We have used the photoresponsivity as a measure to investigate optical properties because it depends on both carrier lifetime and mobility. The photoresponsivity of $BaSi_2$ changes markedly depending on the Ba-to-Si deposition rate ratio (R_{Ba}/R_{Si}) during molecular beam epitaxy (MBE).[30] The photoresponsivity of $BaSi_2$ films grown under Si-rich conditions increased with a decrease in R_{Ba}/R_{Si} and reached a maximum at $R_{Ba}/R_{Si} = 1.2$ when grown at 650 °C.[25] This value is approximately three times higher than that previously reported for samples grown at 580 °C. In contrast to our prediction, however, the crystalline quality of grown layers degraded. The full width at half maximum (FWHM) of the $BaSi_2$ 600 peak measured by ω-scan X-ray rocking curves significantly increased from 0.77° to 5.47°. Therefore, much greater photoresponsivity enhancement can be expected by improving the *a*-axis crystal orientation of $BaSi_2$ films. However, it is not presently clear why the *a*-axis crystal orientation degrades for $BaSi_2$ films grown under Si-rich conditions.

In this work, we perform cross-sectional transmission electron microscopy (X-TEM) observation and defect characterization on the $BaSi_2$ films grown under Si-rich conditions. We then discuss the growth model of $BaSi_2$ layers based on the X-TEM results. Finally, we propose a growth technique, namely, a three-step growth method, to make the Ba-to-Si atomic ratio uniform throughout the entire grown layers, which can be applicable for the growth of other silicides.

II. EXPERIMENTAL METHOD

An ion-pumped MBE system equipped with an electron-beam evaporation source was used for high-purity (10N) Si and a standard Knudsen cell was utilized for low-purity (3N) Ba. For photoresponsivity measurements, we used a Czochralski (CZ) n^+-Si(111) substrate (resistivity $\rho < 0.01\ \Omega$ cm) to ensure that the contribution of photogenerated carriers in the Si substrate to the measured photoresponsivity was negligibly small. Before growing the films, the Si substrates were cleaned by the standard procedure found by Radio Corporation of America, followed by thermal cleaning (TC) at 900 °C for 30 min in an ultrahigh vacuum chamber to remove the protective oxide layer on the surface. For DLTS measurements, CZ n-Si(111) substrates ($\rho = 1$–$4\ \Omega$ cm) were used to form $BaSi_2$/Si heterojunction diodes. In this case, the Si substrates underwent TC at 800 °C for 40 min in addition to the simultaneous deposition of a 1-nm-thick Si layer. With this technique, the defect density in the n-Si region close to the $BaSi_2$/Si interface becomes less than 10^{11} cm^{-3}.[31] For epitaxial growth of $BaSi_2$ films, we evaporated Ba onto the heated Si substrate at $T_S = 500$ °C to form a 5-nm-thick $BaSi_2$ template layer by reactive deposition epitaxy (RDE). This layer acts as a seed for the growth of subsequent layers.[32] In the RDE process, the Ba deposition rate, R_{Ba}, was fixed at 1 nm/min. Next, we grew 500-nm-thick $BaSi_2$ epitaxial layers by MBE at $T_S = 650$ °C. During the MBE growth, R_{Si} was fixed at 0.9 nm/min and R_{Ba} was varied from 0.3 to 4.2 nm/min, giving a variation of R_{Ba}/R_{Si} from 0.4 to 4.7. We also examined a three-step growth method that evolved from a conventional two-step growth method. After RDE, we prepared a 180-nm-thick Ba-rich $BaSi_2$ film ($R_{Ba}/R_{Si} = 4.0$), followed by a 320-nm-thick Si-rich $BaSi_2$ ($R_{Ba}/R_{Si} = 1.2$) layer by MBE. The deposited film thicknesses were set so that the Ba-to-Si atomic ratio in total became stoichiometric. We then formed a 3-nm-thick a-Si capping layer *in situ* at 180 °C, which acted as a surface passivation layer.[33–35] Sample preparation details are shown in Table I. Finally, indium-tin oxide (ITO) electrodes with a diameter of 1 mm and a thickness of 80 nm were sputtered onto the surface, and Al electrodes were formed on the entire back surface.

X-TEM observations were performed using FEI Tecnai Osiris operated at 200 kV, equipped with an energy dispersive X-ray spectrometer (EDX) and a high-angle annular dark-field scanning transmission electron microscopy (HAADF-STEM) system with a probe diameter of ~1 nm. The cross-sectional TEM sample was prepared by the conventional focused ion beam method. X-ray diffraction (XRD; Rigaku Smart Lab) analyses were used to characterize the

TABLE I. Sample preparation details. Si substrate and values of R_{Ba}/R_{Si} for first and second MBE-grown $BaSi_2$ layers. Total thickness of $BaSi_2$ is approximately 500 nm. FWHM values of a $BaSi_2$ 600 peak using ω-scan x-ray rocking curves are also shown.

Sample	Si substrate	R_{Ba}/R_{Si} (1st MBE)	R_{Ba}/R_{Si} (2nd MBE)	FWHM of a $BaSi_2$ 600 peak
A	CZ n^+-Si(111), $\rho < 0.01\ \Omega$ cm	0.4	…	…
B	CZ n^+-Si(111), $\rho < 0.01\ \Omega$ cm	0.9	…	…
C	CZ n^+-Si(111), $\rho < 0.01\ \Omega$ cm	1.2	…	5.47
D	CZ n^+-Si(111), $\rho < 0.01\ \Omega$ cm	1.5	…	2.24
E	CZ n^+-Si(111), $\rho < 0.01\ \Omega$ cm	2.3	…	0.40
F	CZ n^+-Si(111), $\rho < 0.01\ \Omega$ cm	3.7	…	0.20
G	CZ n^+-Si(111), $\rho < 0.01\ \Omega$ cm	4.7	…	0.22
H	CZ n-Si(111), $\rho = 1$–$4\ \Omega$ cm	1.2	…	…
I	CZ n^+-Si(111), $\rho < 0.01\ \Omega$ cm	1.2	4.0	0.39
J	CZ n-Si(111), $\rho = 1$–$4\ \Omega$ cm	1.2	4.0	…

crystalline quality of the grown layers. Epitaxial growth of *a*-axis-oriented $BaSi_2$ was confirmed from the θ–2θ XRD patterns. The FWHM of the $BaSi_2$ 600 peak was measured from ω-scan X-ray rocking curves to evaluate the *a*-axis orientation of the $BaSi_2$ epitaxial films. DLTS was carried out using a 1 MHz capacitance vs voltage (*C*-*V*) meter (HP 4280A). The rate window was varied between 1 and 512 ms. Solar cell performance was evaluated using a mask with a 1-mm-diameter hole under AM1.5 conditions at 25 °C. Photoresponsivity was evaluated with the use of a lock-in technique with a xenon lamp and a 25-cm-focal-length single monochromator (Bunko Keiki SM-1700A and RU-60N). The light intensity was calibrated with a pyroelectric sensor (Melles Griot 13PEM001/J). Hall measurements were conducted for $BaSi_2$ films grown on float-zone high-ρ n- or p-Si(111) substrates ($\rho > 1000\,\Omega$ cm). All measurements were carried out at room temperature.

III. RESULTS AND DISCUSSION

A. Precipitation of excess Si atoms grown under Si-rich conditions

First, the origin of *a*-axis orientation deterioration for $BaSi_2$ films grown under Si-rich conditions was investigated using X-TEM. Figure 1 shows X-TEM images of sample C grown with $R_{Ba}/R_{Si} = 1.2$. We chose sample C among samples A–G because it showed the highest photoresponsivity ever achieved for $BaSi_2$ films grown by the two-step growth method.[25] Figures 1(a)–1(d) are a bright-field (BF) TEM image, high-angle annular dark-field scanning (HAADF) image, EDX mapping of Ba, and EDX mapping of Si, respectively. As shown in Figs. 1(a)–1(d), the $BaSi_2$/Si interface was distinctly rough with a height of 0.2–0.3 μm. The broken lines indicate the position of the initial Si substrate surface before growth. We can see that the Si region exists above the initial Si surface. Figures 1(e) and 1(f), respectively, show the details of the HAADF and EDX images of the rectangular region in Fig. 1(b) just below the $BaSi_2$ layer. From these images, we can state that excess Si atoms in the $BaSi_2$ layer diffused out to the $BaSi_2$/Si interface during MBE growth and precipitated there. Such precipitated Si layers cause the rough interfaces shown in Figs. 1(a)–1(d), leading to the deterioration of the *a*-axis crystal orientation of $BaSi_2$ epitaxial films. Figures 1(g) and 1(h) show the BF-TEM image and a selected-area electron diffraction (SAED) pattern taken for the area shown by the yellow broken circle in Fig. 1(g), respectively. Diffraction spots due to c-Si, marked by yellow circles, make a line as shown in Fig. 1(h), which is not parallel to a white broken line joining diffraction spots of $BaSi_2$. These results verify the *a*-axis orientation deterioration for $BaSi_2$ films. Similar precipitation of excess Si was reported upon the growth of $BaSi_2$ on Ge[36] and $FeSi_2$ films on Si by MBE.[37]

We next investigated the defect properties around the $BaSi_2$/Si interface in sample H by DLTS. DLTS is a powerful method for the investigation of defect densities and their energy levels.[38] In DLTS measurements, a forward filling pulse voltage V_P was set at 0.5 V, and with the pulse width t_{pw} at 50 ms, the reverse bias voltage V_R was varied as −1.0, −0.5, and −0.1 V. As shown in Fig. 2(a), an upward facing peak caused by minority-carrier traps was observed at around 125 K at $V_R = -1.0$ V. This trap is considered to be the same as that reported previously[24] and is interpreted to originate

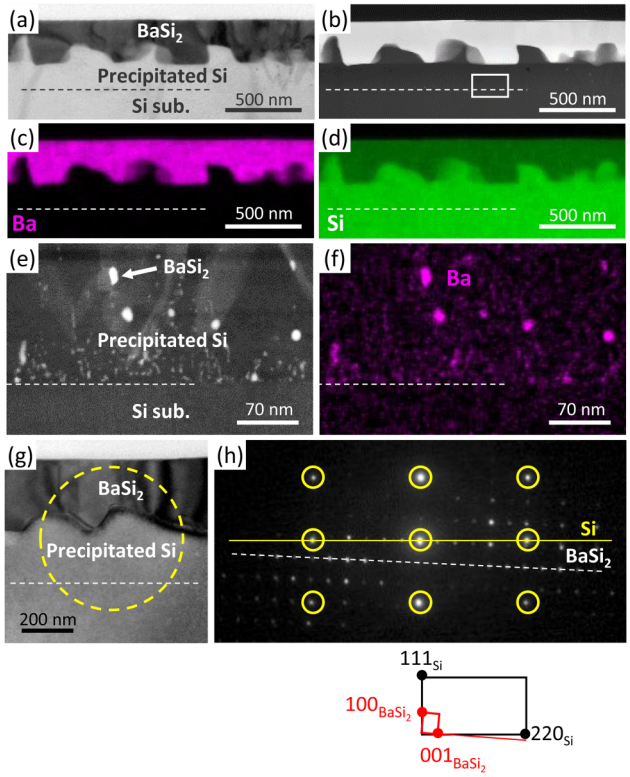

FIG. 1. Cross-sectional TEM observation of $BaSi_2$ films by a two-step growth method under Si-rich conditions (sample C). (a) Bright-field (BF) TEM image. (b) HAADF image. EDX elemental mappings for (c) Ba and (d) Si atoms. (e) HAADF image and (f) EDX mapping for Ba atoms in the Si layer marked by a rectangular region in (b), located between $BaSi_2$ and Si substrate. (g) BF-TEM image and (h) SAED pattern taken from the yellow circle in (g) along Si[11$\bar{2}$].

from Si vacancies. Deep minority-carrier traps have a detrimental impact on the solar cell performance. The downward facing peaks caused by majority-carrier traps were detected over a wide temperature range of 100–200 K at $V_R = -0.1$ V, wherein the magnitude of V_R was small and thus the $BaSi_2$/Si interface was evaluated. Note that measured broad peaks in the DLTS profiles suggest the presence of several kinds of defect levels in the grown films. We next investigated the carrier filling properties for these interface defects by modulating t_{pw}. We changed t_{pw} from 1 to 200 ms and measured the change in capacitance $|\Delta C|$ at 187.5 K, as shown in Fig. 2(b). The DLTS signal $|\Delta C|$ increased gradually as t_{pw} increased from 1 to 200 ms in Fig. 2(c). This is typical in extended defects, wherein the amplitude of the DLTS signal is given by[39–41]

$$\Delta C \propto \ln(t_{pw}). \quad (1)$$

Thus, we interpret the detected interface defects as extended defects originating from precipitated Si layers. These results make it clear that excess Si atoms which diffused out from $BaSi_2$ films

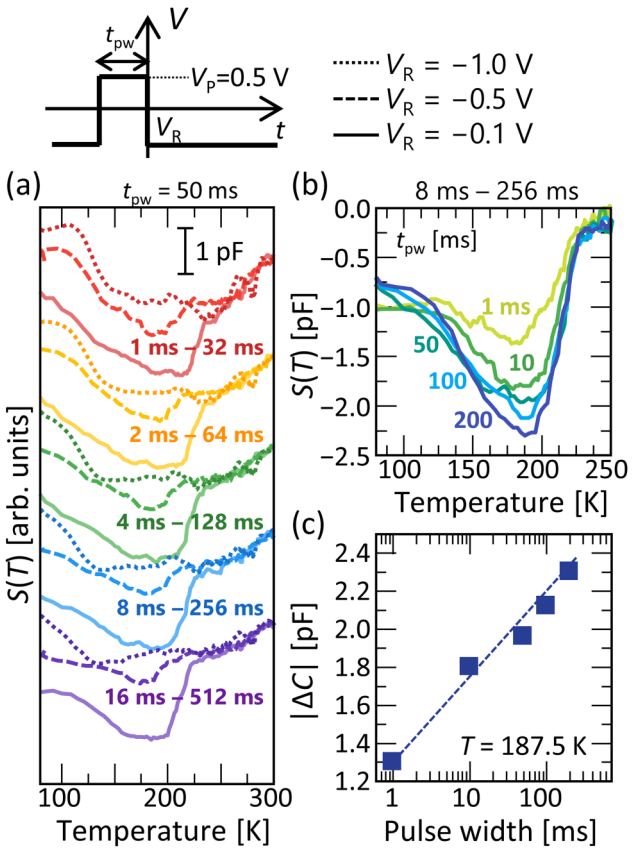

FIG. 2. (a) DLTS profiles of $BaSi_2$ films (sample H) by a two-step growth method measured at V_P = 0.5 V and t_{pw} = 50 ms. V_R was varied as −1.0, −0.5, and −0.1 V. The rate window was varied as 1–32, 2–64, 4–128, 8–256, and 16–512 ms. (b) DLTS profiles obtained at different t_{pw} values from 1 to 200 ms. (c) Dependence of the DLTS signal ΔC on pulse width t_{pw}, measured at 187.5 K. A straight broken line is a guide to the eye.

grown under Si-rich conditions precipitated under the $BaSi_2$ films, and such Si layers, which contain extended defects, degraded the *a*-axis orientation of the $BaSi_2$ epitaxial films. To solve these problems, we propose a growth method for $BaSi_2$ epitaxial films, the three-step growth method, to achieve a stoichiometric $BaSi_2$ film when grown even under Si-rich conditions while suppressing the precipitation of excess Si.

B. Effect of a three-step growth method

A schematic of the three-step growth method is shown in Fig. 3. After RDE (first layer), we prepared a 180-nm-thick $BaSi_2$ second layer grown under Ba-rich conditions (R_{Ba}/R_{Si} = 4.0) to achieve *a*-axis crystal orientation, followed by a 320-nm-thick $BaSi_2$ third layer grown under Si-rich conditions (R_{Ba}/R_{Si} = 1.2). We anticipate that the excess Si atoms in the third layer diffuse out to the second layer and may fill V_{Si} there so that stoichiometry is achieved in the entire film. The layer thicknesses of the second and

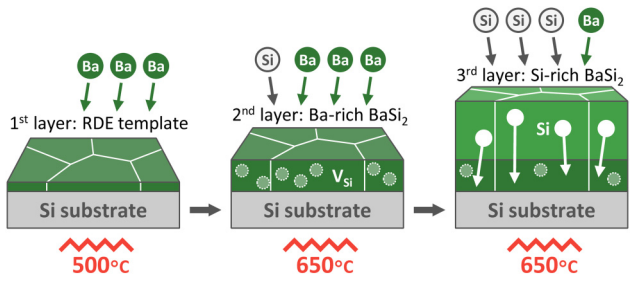

FIG. 3. Schematic image of a three-step growth method.

the third layers were determined such that stoichiometry may be achieved when all the excess Si atoms in the third layer diffuse to the second layer. In this work, we compared sample I, prepared by this method (R_{Ba}/R_{Si} = 1.2 + 4.0), with samples A–G grown with various values of R_{Ba}/R_{Si} by the two-step growth method.

Figure 4 shows X-TEM images of $BaSi_2$ films, sample I, grown by the three-step growth method. Figure 4(a) shows the HAADF image. Compared to the rough interface shown in Fig. 1(a), the interface was quite smooth, showing that the precipitation of Si was significantly suppressed. Figures 4(b)–4(d) are the SAED patterns taken for regions SAED1–3 in Fig. 4(a), respectively, reflecting the formation of *a*-axis-oriented $BaSi_2$ epitaxial films. Figures 1(e)–1(g) show EDX mappings of Ba and Si, HAADF image, and EDX line scan along the line in 1(f), respectively. Ba to Si atomic ratios (N_{Ba}/N_{Si}) were almost uniform over the entire $BaSi_2$, as shown in Fig. 4(g). On the basis of these results, we can state that *a*-axis-oriented $BaSi_2$ epitaxial films with a flat interface and a uniform N_{Ba}/N_{Si} were formed by the three-step growth method. In Fig. 4(a), however, we see grain boundaries (GBs) in $BaSi_2$ films. In our previous work,[10] it was found that *a*-axis-oriented $BaSi_2$ epitaxial films consist of three epitaxial variants that rotate by 120° from each other around the surface normal, and the GBs are mainly composed of $BaSi_2${011} planes from dark-field plane-view TEM observations. From the viewpoint of defect levels, such GBs do not work as electrically active defect sites from the potential distribution measured by Kelvin prove microscopy[42] and by first-principle calculations.[43] However, as we reported in Ref. 44, GBs in $BaSi_2$ act as diffusion paths of impurity dopants. Therefore, $BaSi_2$ films with large grains are preferable for solar cell applications.

Figures 5(a) and 5(b) show the FWHM values of the XRD $BaSi_2$ 600 peak in samples A–G and I, and photoresponsivity spectra of samples C and I. Note that sample C (R_{Ba}/R_{Si} = 1.2) shows the highest photoresponsivity ever achieved for undoped $BaSi_2$ films grown by the two-step growth method.[25] Smaller FWHM values in Fig. 5(a) mean higher *a*-axis orientation of $BaSi_2$ films. The crystal orientation of the $BaSi_2$ films was remarkably improved down to 0.39° for $BaSi_2$ films grown even under Si-rich conditions by using the three-step growth method [Fig. 5(a)]. This result is consistent with the SAED pattern shown in Fig. 4(d). Furthermore, we achieved a significant increase in photoresponsivity in sample I, by approximately five times, compared to sample C (R_{Ba}/R_{Si} = 1.2) [Fig. 5(b)]. Photoresponsivity increases at

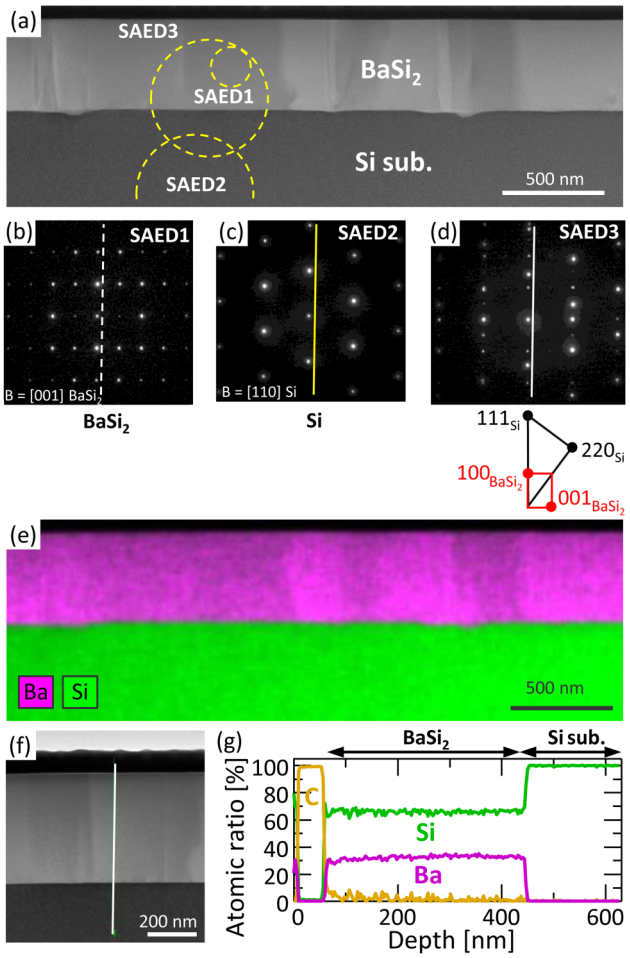

FIG. 4. Cross-sectional TEM characterization of $BaSi_2$ grown by a three-step growth method (sample I). (a) HAADF image. SAED patterns taken from the regions (b) SAED1, (c) SAED2, and (d) SAED3. Lines in (b)–(d) are a guide to the eye. (e) EDX elemental mappings of Ba and Si atoms. (f) Magnified HAADF-STEM image. (g) Si and Ba profiles obtained by a STEM-EDX line scan measurement along the line indicated in (f).

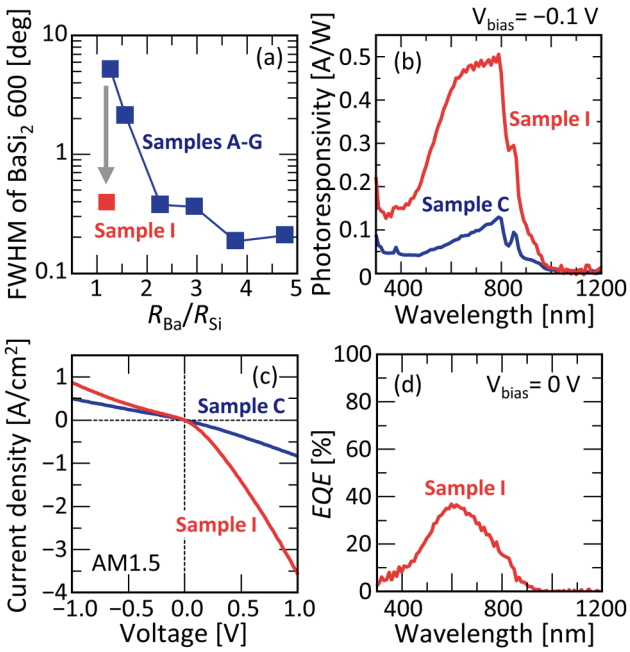

FIG. 5. (a) FWHM values by ω-scan X-ray rocking curves using $BaSi_2$ 600 peak for 0.5-μm-thick $BaSi_2$ films grown by a two-step growth method (samples A–G) and a three-step growth method (sample I). (b) Photoresponse spectra measured under a bias voltage of −0.1 V applied to the front ITO electrode with respect to the back Al electrode. (c) *J-V* characteristics of samples C and I, lightly-p-$BaSi_2$/n-Si solar cells, measured under AM1.5 illumination. (d) *EQE* spectrum of sample I, a lightly-p-$BaSi_2$/n-Si solar cell.

wavelengths shorter than 1000 nm, meaning that carriers photogenerated mostly in the $BaSi_2$ contribute to the photoresponsivity, and reached 0.5 A/W at a wavelength of 800 nm under a bias voltage of −0.1 V. This corresponds to an external quantum efficiency above 90%. Based on these results, it can be stated that we realized $BaSi_2$ light absorbing layers satisfying both of the highly *a*-axis crystal orientation and increased photoresponsivity. Figures 5(c) and 5(d) show the current density vs voltage (*J-V*) characteristics of samples C and I, p-$BaSi_2$/n^+-Si heterojunction diodes under AM1.5 illumination. The p-type conductivity of grown layers was confirmed by the capacitance vs voltage (*C-V*) characteristics described later. As shown in Fig. 5(c), the rectifying *J-V* characteristic was obtained for sample I, not for sample C. In our previous report, we had not yet achieved such rectifying properties in p-$BaSi_2$/n^+-Si diodes. This is because of the presence of defects formed around the $BaSi_2$/Si interfaces, especially formed on heavily doped Si(111) substrates such as n^+-Si(111) substrate.[24] Figure 5(d) shows the external quantum efficiency spectrum of sample I, wherein a separation of photogenerated carriers by the built-in electric field spreading in the p-$BaSi_2$ region was achieved.

We conducted electrical characterizations of $BaSi_2$ films (sample I) grown by the three-step growth method by *C-V* measurement, Hall measurement, and DLTS. To compare with previous results,[24] we prepared another sample formed on an n-Si(111) substrate ($\rho = 1$–$4\ \Omega$ cm), sample J. We found that the conduction types differ between the two samples. This is because the conductivity type of undoped $BaSi_2$ films is very sensitive to N_{Ba}/N_{Si}.[30] From the results of the Hall measurement, $BaSi_2$ films in sample I were p-type, and the hole concentration was $p = 1.1 \times 10^{16}\ cm^{-3}$. However, $BaSi_2$ films in sample J were n-type, and the electron concentration was $n = 4.8 \times 10^{15}\ cm^{-3}$. The carrier type of $BaSi_2$ was also confirmed from the built-in potential (V_{bi}) obtained from the *C-V* characteristics, as shown in Fig. 6(a), wherein the positions of the Fermi level E_F, conduction band minimum E_C, and valence band maximum E_V of $BaSi_2$ and Si are presented with respect to the vacuum level E_{VAC}. The electron affinity of $BaSi_2$ was measured to be approximately 3.2 eV.[45] In the case of p-$BaSi_2$, the E_F of p-$BaSi_2$ is located close to that of n^+-Si, and thereby the V_{bi} should

be small. The measured V_{bi} was 0.09 V for sample I. In the case of n-$BaSi_2$, the difference in E_F between n-$BaSi_2$ and n-Si is large and the V_{bi} should be large. The measured V_{bi} was 0.7 V for sample J. These results suggest that we need dopant impurities in the order of 10^{16} cm^{-3} to fix the carrier type of undoped $BaSi_2$ films.

Figures 6(b) and 6(c) show DLTS profiles of samples I and J, respectively. V_P was set at 0 V and −0.5 V, respectively, t_{pw} was 50 ms, and V_R was varied as −1.0, −0.5, and −0.1 V for sample I. In both cases, two downward facing peaks are present, meaning majority-carrier traps were detected in the region of 100–200 K. Please note that upward facing peaks due to minority-carrier traps were not detected, whereas they were detected in sample C, grown by the two-step growth method [Fig. 2(a)]. In addition, the DLTS profiles became much narrower than those in Fig. 2(a) and those previously reported for $BaSi_2$ films,[23,24] although the DLTS profile in Fig. 6(c) can be reconstructed by two Gaussian curves peaking at E1 and E2. Narrower DLTS profiles suggest the decrease in kind of defects in the grown films, showing that the crystal quality of grown $BaSi_2$ films was improved drastically by the three-step growth method. Figure 6(d) shows Arrhenius plots to find defect levels in samples I and J. The electron trap levels (E1 and E2), working as majority-carrier traps, agree with the levels obtained from the temperature dependence of the resistivity of polycrystalline n-$BaSi_2$ bulk.[46] In addition, the trap level E1 is close to the already reported defect level.[24] The respective defect densities of E1, E2, and hole trap levels (H1 and H2) are 4.7×10^{14} cm^{-3}, 1.1×10^{14} cm^{-3}, 8.3×10^{13} cm^{-3}, and 1.7×10^{14} cm^{-3}. From these results, we conclude that the three-step growth method enables us to produce highly crystalline $BaSi_2$ films without minority-carrier traps compared to those by the conventional two-step growth method, thereby achieving a high photoresponsivity. Such distinct peaks in the DLTS profiles, however, show the existence of remaining defects in $BaSi_2$ grown by the three-step growth method. They should be decreased much further or inactivated in the near future.

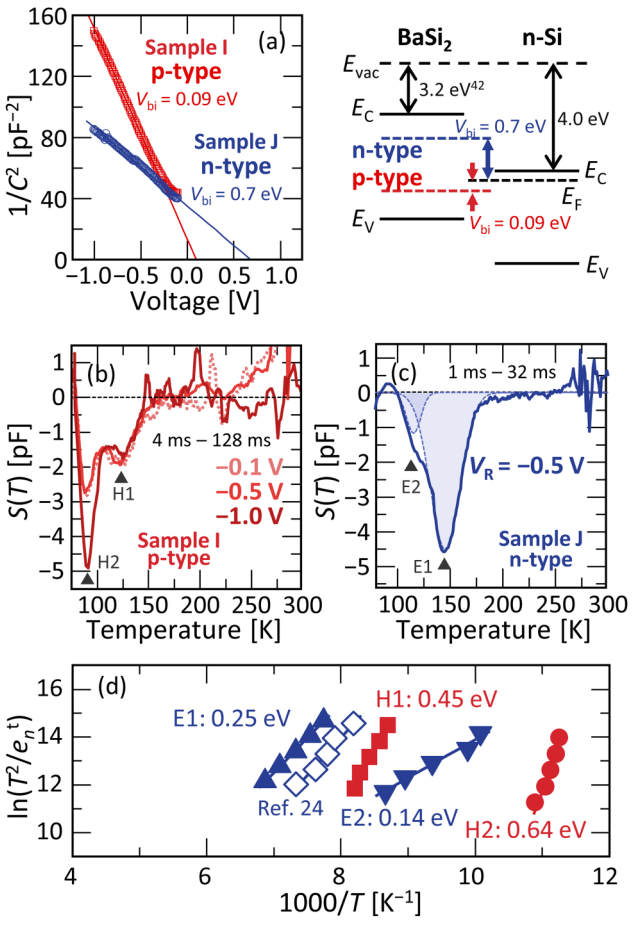

FIG. 6. (a) $1/C^2$ vs V plots for 0.5-μm-thick $BaSi_2$ grown by a three-step growth method. Band alignment of $BaSi_2$ and Si with respect to the vacuum level, E_{vac}. (b) DLTS profiles of p-type $BaSi_2$ films (sample I) at V_P = 0.5 V and t_{pw} = 50 ms. V_R was varied as −1.0, −0.5, and −0.1 V. (c) DLTS profiles of n-type $BaSi_2$ films (sample J) at V_P = 0 V and t_{pw} = 50 ms. V_R was set at −0.5 V. (d) Arrhenius plots for electron trap levels (E1, E2) and hole trap levels (H1, H2). Data reprinted from permissions from Yamashita *et al.*, Jpn. J. Appl. Phys. **57**, 075801 (2018). Copyright (2018) The Japan Society of Applied Phyiscs.[24]

Finally, we mention the availability of this three-step growth method to the formation of other silicides. From the Ba-Si phase diagram,[47,48] $BaSi_2$ is a line compound, and there is no other Ba-Si phase next to Si, meaning that $BaSi_2$ is stable with the presence of crystalline Si. This is a reason why $BaSi_2$ films grown under Si-rich conditions (wherein precipitation of excess Si occurs) can show better optical and electrical properties than those under Ba-rich conditions (wherein a small amount and thereby undetected other phases such as BaSi and point defects such as V_{Si} are likely to exist). Therefore, we speculate that the proposed three-step growth method can be available to those systems that have a phase diagram similar to Ba-Si.

IV. CONCLUSION

We fabricated 500-nm-thick $BaSi_2$ films at 650 °C by MBE and investigated the crystalline quality and defect properties of $BaSi_2$ bulk and $BaSi_2$/Si interface regions by X-TEM, DLTS, and photoresponse spectroscopy. X-TEM showed that Si atoms diffused from the $BaSi_2$ layers to the $BaSi_2$/Si interface and excess Si precipitated there. DLTS revealed that precipitated Si caused extended defects. To suppress such Si precipitation, we proposed a three-step growth method. By this method, the $BaSi_2$/Si interface smoothness and *a*-axis orientation of $BaSi_2$ films were improved drastically, and therefore the photoresponsivity was enhanced markedly (by a factor of five). The DLTS profiles became much narrower in $BaSi_2$ films grown by the three-step growth method, meaning that the type of defect levels in $BaSi_2$ films decreased compared to those by the two-step growth method. Furthermore, minority-carrier traps were not detected. We, therefore, conclude that we realized $BaSi_2$ light absorbing layers that satisfy both high crystal orientation and high photoresponsivity.

ACKNOWLEDGMENTS

This work was financially supported by JSPS KAKENHI (Grant Nos. 17K18865 and 18H03767) and JST MIRAI. One of the

authors (Y.Y.) was financially supported by a Grant-in-Aid for JSPS Fellows (No. 19J21372).

REFERENCES

[1]K. Yoshikawa, H. Kawasaki, W. Yoshida, T. Irie, K. Konishi, K. Nakano, T. Uto, D. Adachi, M. Kanematsu, H. Uzu, and K. Yamamoto, Nat. Energy **2**, 17032 (2017).
[2]W. Shockley and H. J. Queisser, J. Appl. Phys. **32**, 510 (1961).
[3]Press Release, Fraunhofer Institute for Solar Energy Systems, 1 December 2014.
[4]M. Imai and T. Hirano, J. Alloys Compd. **224**, 111 (1995).
[5]T. Suemasu and N. Usami, J. Phys. D **50**, 023001 (2017).
[6]K. Toh, T. Saito, and T. Suemasu, Jpn. J. Appl. Phys. **50**, 068001 (2011).
[7]D. B. Migas, V. L. Shaposhnikov, and V. E. Borisenko, Phys. Status Solidi B **244**, 2611 (2007).
[8]M. Kumar, N. Umezawa, and M. Imai, J. Appl. Phys. **115**, 203718 (2014).
[9]M. Kumar, N. Umezawa, and M. Imai, Appl. Phys. Express **7**, 071203 (2014).
[10]M. Baba, K. Toh, K. Toko, N. Saito, N. Yoshizawa, K. Jiptner, T. Sekiguchi, K. O. Hara, N. Usami, and T. Suemasu, J. Cryst. Growth **348**, 75 (2012).
[11]M. A. Khan, K. O. Hara, W. Du, M. Baba, K. Nakamura, M. Suzuno, K. Toko, N. Usami, and T. Suemasu, Appl. Phys. Lett. **102**, 112107 (2013).
[12]M. A. Khan, K. Nakamura, W. Du, K. Toko, N. Usami, and T. Suemasu, Appl. Phys. Lett. **104**, 252104 (2014).
[13]M. Kobayashi, Y. Matsumoto, Y. Ichikawa, D. Tsukada, and T. Suemasu, Appl. Phys. Express **1**, 051403 (2008).
[14]M. Kumar, N. Umezawa, W. Zhou, and M. Imai, J. Mater. Chem. A **5**, 25293 (2017).
[15]R. A. McKee and F. J. Walker, Appl. Phys. Lett. **63**, 2818 (1993).
[16]S. Yachi, R. Takabe, H. Takeuchi, K. Toko, and T. Suemasu, Appl. Phys. Lett. **109**, 072103 (2016).
[17]D. Tsukahara, S. Yachi, H. Takeuchi, R. Takabe, W. Du, M. Baba, Y. Li, K. Toko, N. Usami, and T. Suemasu, Appl. Phys. Lett. **108**, 152101 (2016).
[18]T. Deng, T. Sato, Z. Xu, R. Takabe, S. Yachi, Y. Yamashita, K. Toko, and T. Suemasu, Appl. Phys. Express **11**, 062301 (2018).
[19]T. Suemasu, Jpn. J. Appl. Phys. **54**, 07JA01 (2015).
[20]K. Kodama, R. Takabe, S. Yachi, K. Toko, and T. Suemasu, Jpn. J. Appl. Phys. **57**, 031202 (2018).
[21]K. Kodama, R. Takabe, T. Deng, K. Toko, and T. Suemasu, Jpn. J. Appl. Phys. **57**, 050310 (2018).
[22]K. Kodama, Y. Yamashita, K. Toko, and T. Suemasu, Appl. Phys. Express **12**, 041005 (2019).
[23]H. Takeuchi, W. Du, M. Baba, R. Takabe, K. Toko, and T. Suemasu, Jpn. J. Appl. Phys. **54**, 07JE01 (2015).
[24]Y. Yamashita, T. Sato, M. Emha Bayu, K. Toko, and T. Suemasu, Jpn. J. Appl. Phys. **57**, 075801 (2018).
[25]Y. Yamashita, Y. Takahara, T. Sato, K. Toko, A. Uedono, and T. Suemasu, Appl. Phys. Express **12**, 055506 (2019).
[26]T. Sato, H. Hoshida, R. Takabe, K. Toko, Y. Terai, and T. Suemasu, J. Appl. Phys. **124**, 025301 (2018).
[27]T. Sato, C. Lombard, Y. Yamashita, Z. Xu, L. Benincasa, K. Toko, S. Gambarelli, and T. Suemasu, Appl. Phys. Express **12**, 061005 (2019).
[28]Z. Xu, K. Gotoh, T. Deng, T. Sato, R. Takabe, K. Toko, N. Usami, and T. Suemasu, AIP Adv. **8**, 055306 (2018).
[29]Z. Xu, D. A. Shohonov, A. B. Filonov, K. Gotoh, T. Deng, S. Honda, K. Toko, N. Usami, D. B. Migas, V. E. Borisenko, and T. Suemasu, Phys. Rev. Mater. **3**, 065403 (2019).
[30]R. Takabe, T. Deng, K. Kodama, Y. Yamashita, T. Sato, K. Toko, and T. Suemasu, J. Appl. Phys. **123**, 045703 (2018).
[31]Y. Yamashita, S. Yachi, R. Takabe, T. Sato, M. Emha Bayu, K. Toko, and T. Suemasu, Jpn. J. Appl. Phys. **57**, 025501 (2018).
[32]Y. Inomata, T. Nakamura, T. Suemasu, and F. Hasegawa, Jpn. J. Appl. Phys. **43**, 4155 (2004).
[33]R. Takabe, K. O. Hara, M. Baba, W. Du, N. Shimada, K. Toko, N. Usami, and T. Suemasu, J. Appl. Phys. **115**, 193510 (2014).
[34]R. Takabe, S. Yachi, W. Du, D. Tsukahara, H. Takeuchi, K. Toko, and T. Suemasu, AIP Adv. **6**, 085107 (2016).
[35]R. Takabe, H. Takeuchi, W. Du, K. Ito, K. Toko, S. Ueda, A. Kimura, and T. Suemasu, J. Appl. Phys. **119**, 165304 (2016).
[36]R. Takabe, S. Yachi, D. Tsukahara, K. Toko, and T. Suemasu, Jpn. J. Appl. Phys. **56**, 05DB02 (2017).
[37]A. Schöpke, B. Selle, I. Sieber, G.-U. Reinsperger, P. Stauβ, K. Herz, and M. Powalla, Fresen. J. Anal. Chem. **358**, 322 (1997).
[38]D. V. Lang, J. Appl. Phys. **45**, 3023 (1974).
[39]S.-H. Wei, S. B. Zhang, and A. Zunger, Appl. Phys. Lett. **72**, 3199 (1998).
[40]S.-H. Wei and A. Zunger, J. Appl. Phys. **78**, 3846 (1995).
[41]T. Wosinski, J. Appl. Phys. **65**, 1566 (1989).
[42]M. Baba, S. Tsurekawa, K. Watanabe, W. Du, K. Toko, K. O. Hara, N. Usami, T. Sekiguchi, and T. Suemasu, Appl. Phys. Lett. **103**, 142113 (2013).
[43]M. Baba, M. Kohyama, and T. Suemasu, J. Appl. Phys. **120**, 085311 (2016).
[44]K. Nakamura, M. Baba, K. M. Ajmal, W. Du, M. Sasase, K. O. Hara, N. Usami, K. Toko, and T. Suemasu, J. Appl. Phys. **113**, 053511 (2013).
[45]T. Suemasu, K. Morita, M. Kobayashi, M. Saida, and M. Sasaki, Jpn. J. Appl. Phys. **45**, L519 (2006).
[46]T. Nakamura, T. Suemasu, K.-I. Takakura, F. Hasegawa, A. Wakahara, and M. Imai, Appl. Phys. Lett. **81**(6), 1032–1034 (2002).
[47]M. Pani and A. Palenzona, J. Alloys Compd. **454**, L1 (2008).
[48]S. Kishino, T. Imai, T. Iida, Y. Nakaishi, M. Shinada, Y. Takanashi, and N. Hamada, J. Alloys Compd. **428**, 22 (2007).